analytical chemistry

Article

pubs.acs.org/ac

Three-Dimensional Carbon Interdigitated Electrode Arrays for Redox-Amplification

Rahul R. Kamath* and Marc J. Madou

Biomedical Engineering, University of California at Irvine, Irvine, California 92697, United States

Mechanical and Aerospace Engineering and Biomedical Engineering, University of California at Irvine, Irvine, California 92697, United States

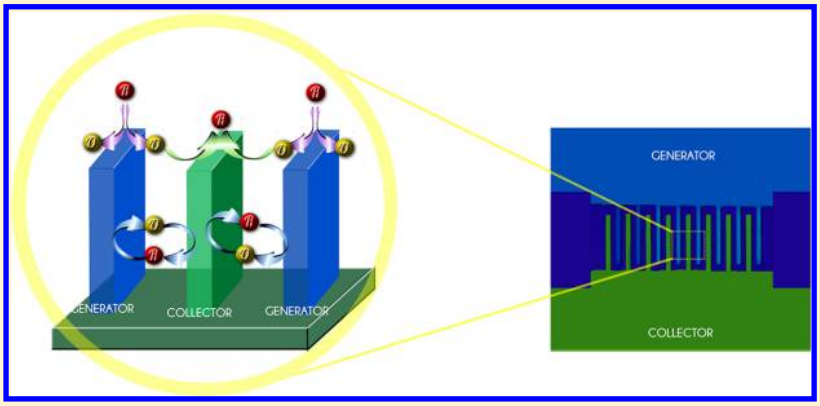

ABSTRACT: Three-dimensional (3D) carbon interdigitated electrode arrays (IDEAs) were fabricated using inexpensive, conventional, UV photolithography of SU-8 with modified exposure and post exposure bake settings followed by pyrolysis in an inert environment. The sensor performance was investigated as a function of both the IDEA digit width/gap ratio and digit height under flow and no flow conditions. We demonstrated a gradual increase in redox amplification with an increase in the IDEA digit width/gap ratio. The highest amplification of 37 was obtained for a width/gap ratio of 1.58 and for an electrode height of 1.1 μm. Redox amplification also increases significantly with an increase in the IDEA height, from a factor of 9 at a 0.22 μm digit height to a factor of 37 at a 1.1 μm height. The effect of potential sweep rates on redox amplification was also investigated. As the sweep rate was decreased from 50 mV/s to 5 mV/s, the collection efficiency increased from 0.92 to 0.97, whereas the amplification increased from 7 to 25. Under flow conditions, the amplification decreases substantially as the cycling of the redox species is impeded by convection, resulting in a drop in collection efficiency. The highest amplification of 37 dropped to 4 for the same electrode at a flow rate of 500 nL/s. Under flow, redox amplification increased with an increase in the IDEA height.

Electrochemical sensors constitute an attractive alternative to optical detection as they offer simpler measurements and can operate in turbid solutions. Furthermore, miniaturizing electrochemical sensors further lowers the requirements on the amount of reagents used, improves the lower limit of detection (LOD),[1] reduces response time, improves its operation in highly resistive media,[2] reduces the footprint of the equipment involved, and is more cost-effective.[3,4] In recent years, microelectromechanical system (MEMS) and nanoelectromechanical system (NEMS) based electrochemical sensors have received much attention for bioelectronics applications due to their ease of use, ability to perform multiparameter biosensing, such as label-free detection of nucleic acid hybridization,[5] and their compatibility with other miniaturized diagnostic tools, such as microfluidic platforms.[6] Genomics, proteomics, and cell analysis are some areas of advanced biomedical research where electrochemical sensing has been pervasive.[7−9] Redox amplification is yet another fascinating application of electrochemical sensing where advancements in micro- and nanofabrication techniques haves brought about significant changes.[10,11]

Redox amplification is one of the most popular applications involving the use of interdigitated electrode arrays (IDEAs) (Figure 1).[12−15] If two adjacent electrodes in an IDEA are closely spaced and biased at different potentials (specific to the redox species of interest), then species undergo oxidation at the electrode with the higher potential (generator) and oxidized species undergo reduction at the electrode with the lower potential (collector) before diffusing out into the bulk of the solution. If the generator and collector electrodes are in close proximity such that adjacent regions with concentration gradients overlap significantly, then the redox couple may cycle multiple times (redox cycling) before the species diffuse out into the bulk solution (shown in Figure 1).[16] This behavior

Received: October 15, 2013
Accepted: February 24, 2014
Published: February 24, 2014

   dx.doi.org/10.1021/ac4033356 | *Anal. Chem.* 2014, 86, 2963−2971

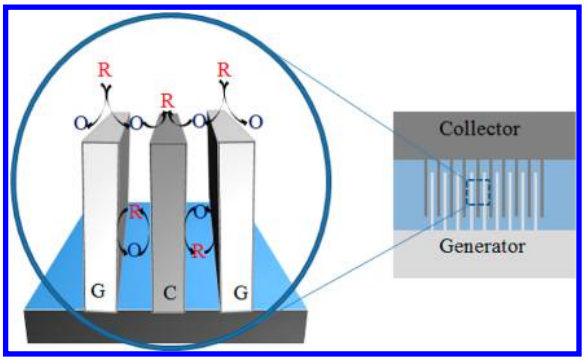

Figure 1. Schematic view of principle of redox cycling in a 3D IDEA. G: Generator; C: Collector. The redox species oxidize at the generator and reduce at the collector multiple times (one cycle is shown here) before diffusing out in the bulk solution.

results in an amplified signal, lowering the limit of detection (LOD) significantly. However, to get a sizable redox amplification factor, discussed later in this work, one needs to operate with electrode gaps in the submicrometer range.[17] The biggest advantage of redox amplification in an IDEA with submicrometer gap spacing is that it allows measurement of extremely small concentrations of an analyte. Furthermore, IDEAs are effective in analyzing extremely small sample volumes. This is possible because an IDEA cycles a redox species multiple times, causing the analyte to regenerate and thereby maintain the concentration of analyte in the bulk for a longer period of time. A single microelectrode cannot maintain the bulk analyte concentration for very long because the analyte is being consumed without regeneration during the electrochemical reaction. This strategy has been explored to detect analytes in an 800 nL sample and obtain a subfemtomolar detection limit using gold planar IDEAs.[18]

In this contribution, we report on a simple, UV photolithography based, batch fabrication technique where SU-8, a negative tone photoresist, is patterned into the desired IDEA geometry. These SU-8 patterns are subsequently pyrolyzed in an inert environment for obtaining three-dimensional (3D) carbon IDEAs (Figure 2). 3D carbon IDEAs, with enhanced redox amplification factors, constitute an inexpensive alternative to the more traditionally used noble metal IDEAs. Redox amplification factors demonstrated here are about 37, the highest reported yet for carbon interdigitated electrodes fabricated using conventional UV photolithography. Different research groups[19,17,20] have focused on achieving high amplification factors (>20) by reducing the gap spacing between the digits of an IDEA whereas very few[15,21] have focused on increasing electrode height for signal enhancement. Even fewer have reported signal enhancement on 3D carbon IDEAs.[22] Dam et al. have reported an amplification factor of ∼70 for 3D IDEAs. However, the Dutch group led by A. Van Den Berg used platinum electrodes which were fabricated using a complex BOSCH process. Our focus here was to improve and expand significantly upon the work done by Heo et al.[22] in developing even taller carbon IDEAs to achieve greater amplification and to investigate the potential sweep rate and flow dependence of the amplification factor. We evaluate the IDEA sensor performance in terms of the redox amplification and collection efficiency (CE) (CE is defined as the ratio of the collector current to the generator current) as a function of the electrode height, width/gap ratio, the potential sweep rate across the electrodes, and a function of flow conditions. Carbon

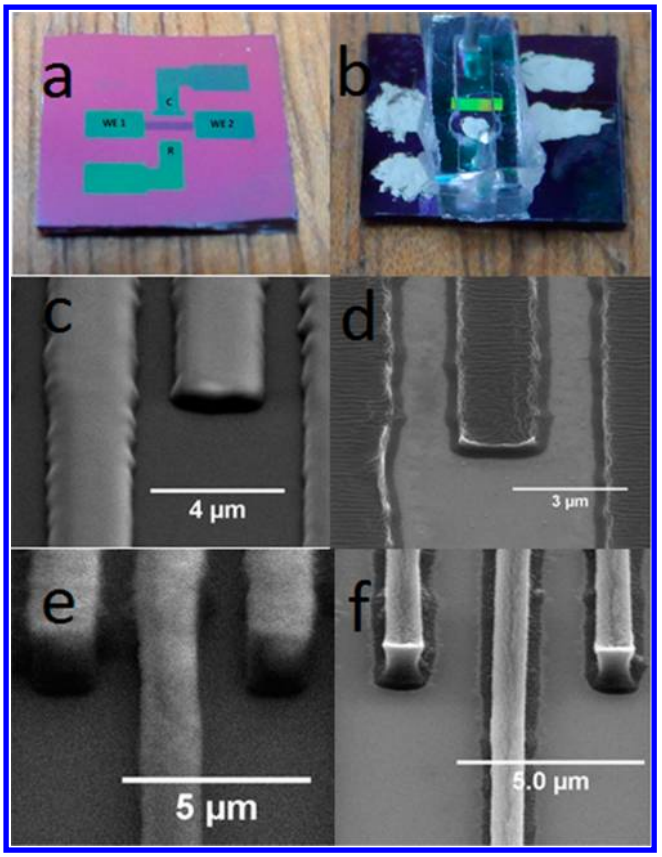

Figure 2. (a) Shows the actual 3D carbon IDEA sensor. WE1 and WE2 are contact pads for the generator and the collector, respectively. C and R are counter and reference electrodes, respectively. (b) Shows the final device with PDMS channels. The reference electrode is coated with Ag/AgCl ink, and contact pads are coated with silver paste for better electrical connection. (c and e) Scanning electron microscopy (SEM) images (tilted view 60°) under 10 000× magnification of SU-8 IDEA patterning before pyrolysis; height = 0.6 and 2.1 μm, respectively. (d and f) Carbon IDEA after pyrolysis; height = 0.22 and 0.59 μm, respectively. Exact width and gap specifications are listed in Tables 1 and 2.

IDEA fabrication not only offers cost advantages but also reduces the number of fabrication steps (for example, the use of an adhesion layer and a lift-off step involved in noble metal IDEA fabrication is avoided), thus increasing the fabrication yield. Moreover, Au/Cr or Au/Ti bilayers, used in conjunction with noble metal IDEAs and when in contact with an electrolyte, constitute a galvanic couple that may lead to corrosion, thereby limiting their long-term application in electrochemical cells. Finally, while metal electrodes exhibit a lower electrical resistance than carbon, they come with all types of unwanted electrochemical side reactions even at low potentials.[23] Carbon, on the other hand, is chemically very stable and comes with a wider stability window than any noble metal. The physiochemical properties of pyrolyzed carbon are comparable to that of glassy carbon.[24] Carbon also exhibits good biocompatibility, low nonspecific adsorption of biomolecules, and low tendency for fouling. As a result, carbon electrodes are the gold standard for studying electrochemical reactions[25] and make for an attractive material for fabricating IDEA electrodes.

dx.doi.org/10.1021/ac4033356 | Anal. Chem. 2014, 86, 2963−2971

MATERIALS AND METHODS

Materials. Analytical reagent grade potassium ferrocyanide ($K_4Fe(CN)_6$) and potassium chloride (Sigma Aldrich) were used in the experiment. SU-8 2000.5, 2002, and 2005 with viscosities 2.49, 7.5, and 45 cSt, respectively, were purchased from Microchem. Inc. MA, USA. Silicon wafers, passivated with a 500 nm oxide layer, were obtained from Noel Technologies, CA, USA. These wafers were used as received for the fabrication process. Our IDEA design was printed on a high resolution, chrome photomask obtained from Photosciences Inc., CA, USA.

Sensor Design, Fabrication, and Characterization. Four different working electrode designs were used. Each generator and collector set consisted of 70 digits, each of them 2 mm long. The four designs included four different digit widths with two gap spacings, as listed in Table 1. The counter and reference electrodes, also made from carbon, were fabricated at a distance of 500 μm on either side of the array. The carbon electrode intended for reference was coated with a droplet of Ag/AgCl ink and allowed to dry before experiments. These designs were photolithographically patterned, employing SU-8 on a Si wafer passivated by a silicon dioxide layer as mentioned above. The patterning was followed by pyrolysis under nitrogen flow. Low viscosity SU-8 was used to produce thin films by spin coating. This was essential to achieve submicrometer gap dimensions during patterning. SU-8 2000.5, SU-8 2002, and SU-8 2005 (viscosities as mentioned above) were spin-coated according to the manufacturer's recommendations to produce films of different thicknesses, as listed in Table 2. SU-8 2000.5 was used to achieve a 0.6 μm height; SU-8 2002 was used to achieve 2.1 and 3.6 μm heights (two layers of SU-8 spin-coat) whereas a 5.1 μm height was obtained using SU-8 2005. The UV exposure was carried out with hard contact between the photomask and the SU-8 coated wafer in a mask aligner (MA56 Karl Suss). It was difficult to achieve complete separation of the generator and collector electrodes using the exposure and post exposure bake (PEB) settings recommended in the Microchem datasheets. Using the recommended exposure dosage and PEB settings (time and temperature) caused IDEAs to merge because, we speculate, the acid generated during exposure diffuses into the unexposed submicrometer gap spacing. To avoid this, the exposure dosage was lowered to 30 mJ/sq·cm to reduce the amount of acid generated and thus to minimize its diffusion across the generator/collector gaps. Keeping the recommended PEB time and temperature caused the SU-8 film to peel off during development due to insufficient adhesion with the substrate. Hence, we modified the PEB time from 1 to 2 min at 95 °C to 90 min at 55 °C to maintain a higher fidelity of the IDEA patterns during development. The lower PEB temperature also helped in reducing the acid diffusion generated in the UV exposure. Similar observations[26] were reported for high resolution fabrication of thin SU-8 film patterns. Summarizing, the required lithography process modifications for our application included a reduction of the exposure dosage and increase in the PEB time (same for all the thicknesses listed in Table 2) to compensate for the lower exposure dosage and thus avoid peeling of patterns during development. The SU-8 patterns obtained after development were pyrolyzed to yield carbon IDEAs. Pyrolysis was performed in an RD Webb Red Mini #40 tube furnace. During the pyrolysis process, cross-linked SU-8 is heated up to 900 °C under a nitrogen flow. The temperature ramp up rate, 10 °C/min in this study, is maintained in such a way that the furnace temperature always remains lower than the glass transition temperature of the SU-8. The details of the pyrolysis process were reported elsewhere.[27] Pyrolysis for thicker SU-8 structures (around 10 μm) results in a vertical shrinkage of approximately 85%.[28] However, as the SU-8 structure height decreases, the vertical shrinkage decreases from 79% at 5.1 μm to 64% at 0.6 μm. The digit width at the base where SU-8 is anchored to the substrate remains the same before and after pyrolysis, irrespective of the original width and height. There is definite lateral shrinkage at the top of the SU-8 structures, but the shrinkage is consistent for all the heights studied: from 64% at a 0.8 μm digit width to 26% at a 2.7 μm digit width. The calculations for the width of electrodes, gaps, and their ratios was done by averaging the measurements at the base and top of the digits.[29]

Carbon IDEA samples were characterized by scanning electron microscopy (SEM) and profilometry to determine the feature dimensions. SEM imaging was carried out on a FEI Quanta 3D FEG system, and profilometry was carried out using a Dektak Profilometer. To obtain SEM images before pyrolysis, SU-8 patterns were sputtered with carbon (up to 5 nm) using an ion beam sputtering system (model: IBS/e from South Bay Technology, USA). The sputtered SU-8 patterns were not pyrolyzed and not used further in this study. Cyclic voltammograms (CVs) and chronoamperograms (CAs) were studied to determine the electrochemical properties of the IDEAs. CV and CA experiments were carried out on an EDAQ Quadstat 164 setup, Chart software v5, and a Waveform Generator ER175. CVs were carried out in a 0.5 M KCl solution containing 1 mM $K_4Fe(CN)_6$ at two different sweep

Table 1. Digits Widths, Gap Spacings, and Height before and after Pyrolysis for the Shortest 3D IDEAs[a]

height	width	gap	width/gap (avg.)
H_{bp} = 0.6, H_{ap} = 0.22	W_b = 0.75	G_b = 0.85	0.47
	W_t = 0.27	G_t = 1.33	
	W_b = 0.86	G_b = 0.94	0.54
	W_t = 0.4	G_t = 1.4	
	W_b = 1.75	G_b = 1.05	0.96
	W_t = 1.0	G_t = 1.8	
	W_b = 2.72	G_b = 1.08	1.66
	W_t = 2.02	G_t = 1.78	
	W_b = 1.75	G_b = 1.25	0.85
	W_t = 1.0	G_t = 2.0	

[a] H_{bp} = height before pyrolysis, H_{ap} = height after pyrolysis. W_b = width at the base, W_t = width at the top. G_b = gap at the base, G_t = gap at the top. All units are in μm except width/gap ratio.

Table 2. Digit Widths and Gap Spacing for Different Heights before and after Pyrolysis[a]

height	width	gap	width/gap (avg.)
H_{bp} = 0.6, H_{ap} = 0.22	W_b = 2.72	G_b = 1.08	1.66
	W_t = 2.02	G_t = 1.78	
H_{bp} = 2.1, H_{ap} = 0.59	W_b = 2.72	G_b = 1.08	1.63
	W_t = 1.99	G_t = 1.81	
H_{bp} = 3.6, H_{ap} = 0.86	W_b = 2.7	G_b = 1.1	1.59
	W_t = 1.96	G_t = 1.84	
H_{bp} = 5.1, H_{ap} = 1.1	W_b = 2.7	G_b = 1.1	1.58
	W_t = 1.95	G_t = 1.85	

[a] All units are in μm except width/gap ratio.

dx.doi.org/10.1021/ac4033356 | Anal. Chem. 2014, 86, 2963−2971

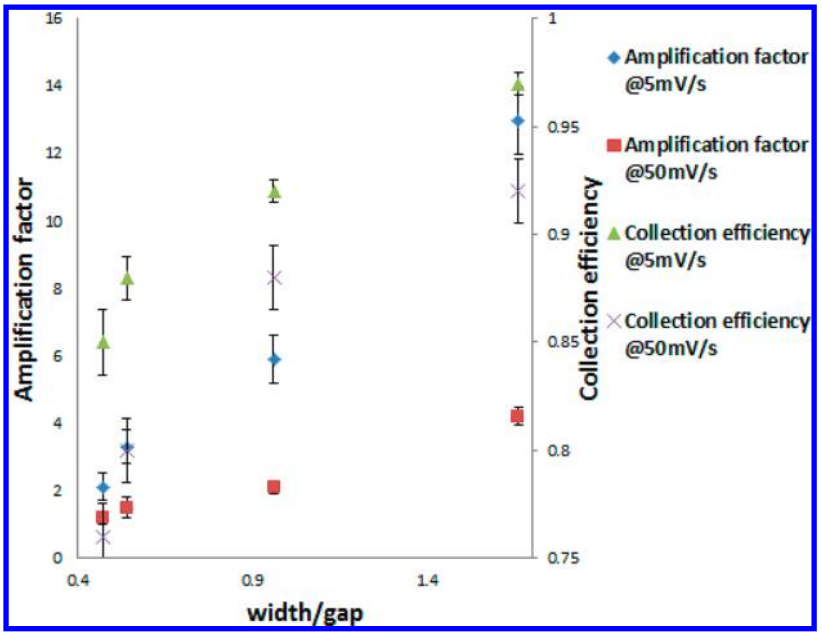

Figure 3. Amplification factor and collection efficiency vs width/gap ratio at a 0.22 μm height under no flow condition. Width/gap ratios are derived from Table 1.

rates of 50 and 5 mV/s. The reference electrode was a pseudoreference of an Ag/AgCl ink droplet (Bio-Logics, USA) coated on the reference carbon electrode and then dried in an oven at 60 °C for 1 h. CV experiments were carried out in single and dual mode. For single mode runs, the collector circuit was kept open and the generator potential was swept between −200 and 600 mV. In dual mode, the generator potential was swept the same as in single mode but the collector was held constant at −250 mV vs the reference electrode. For the CA experiments, the generator was kept at an oxidation potential of 400 mV and the collector was kept at −250 mV, in the case of dual mode. After approximately half a minute of dual mode operation, the collector was disconnected to measure generator current in single mode. The redox amplification factor is calculated as the ratio of the generator current in dual mode to the generator current in single mode, whereas collector efficiency is given by the ratio of collector current to generator current in dual mode.

For steady state experiments, experiments were conducted in a stationary solution. To ensure very little evaporation of the solution during the duration of the experiment, the IDEA was enclosed in a PDMS channel. The PDMS channel ensured that there is little to no evaporation of the solution during the course of the experiments. PDMS channels were crafted using plastic molds carved out on a cutter plotter. The channels were sealed onto the IDEA sensor substrate using a 2:1 mixture of base to curing agent (PDMS precursors, Sylgard, USA). The mixture, used as an adhesive, was allowed to cure at 70 °C overnight. PDMS channels that were 1.5 mm wide and 100 μm high were used for all experiments. The inlet and outlets of the PDMS channels placed over the IDEAs were connected to PTFE tubing for supplying the electrolyte solution to be tested. $K_4Fe(CN)_6$ solution was introduced into the inlet using a syringe pump (World Precision Instruments, USA). For flow experiments, the infusion rate was kept at 500 nL/s, which corresponds to a linear velocity of approximately 3 mm/s for the channel dimensions with the flow orthogonal to the IDEAs. To get rid of any trapped air in the channel, the solution was allowed to flow over the IDEAs for a few seconds before the CA and CV readings were taken.

RESULTS AND DISCUSSION

Signal Enhancement as a Function of Width/Gap Ratio (No Flow). The dependence of redox amplification on the electrode width and electrode gap is known.[17,30] Aoki et al.[16] derived analytically an approximate equation by solving the two-dimensional diffusion equation for reversible redox reactions of soluble species in steady state. This leads to an expression for the limiting current on a planar IDEA in steady state as follows:

$$I_{lim} = mbnFCD\left[0.637\ln\frac{2.55}{x} - 0.19x^2\right] \quad (1)$$

where m is the number of digits in the array, b is the length of each digit, n is the number of electrons involved in the redox reaction, F is Faraday's constant, C is the bulk concentration of the redox molecule of interest, and D is the diffusion coefficient of the same molecule. x in eq 1 is given by $x = g/(W + g)$, where g is the gap between adjacent digits and W is the width of each digit. The electrode height as well as the potential sweep rate was not factored in this expression. When the current in dual mode is divided by the current obtained at the generator in single mode, we get the redox amplification factor, RA. The relationship between redox amplification and collection efficiency, CE, is given as:

$$RA = 1/(1 - CE^2) \quad (2)$$

To evaluate the performance of carbon IDEAs in a stationary solution (no flow), redox amplification factors and collection efficiencies were evaluated for different gaps as well as for different width/gap ratios and different electrode heights. It has been observed by different groups[17,30] that if the electrode width is kept constant, then the amplification factor increases as the gap between the electrodes is reduced. This is because the diffusion path for redox species cycling between IDEA digits is reduced. Figure 3 shows the redox amplification and collection

dx.doi.org/10.1021/ac4033356 | Anal. Chem. 2014, 86, 2963−2971

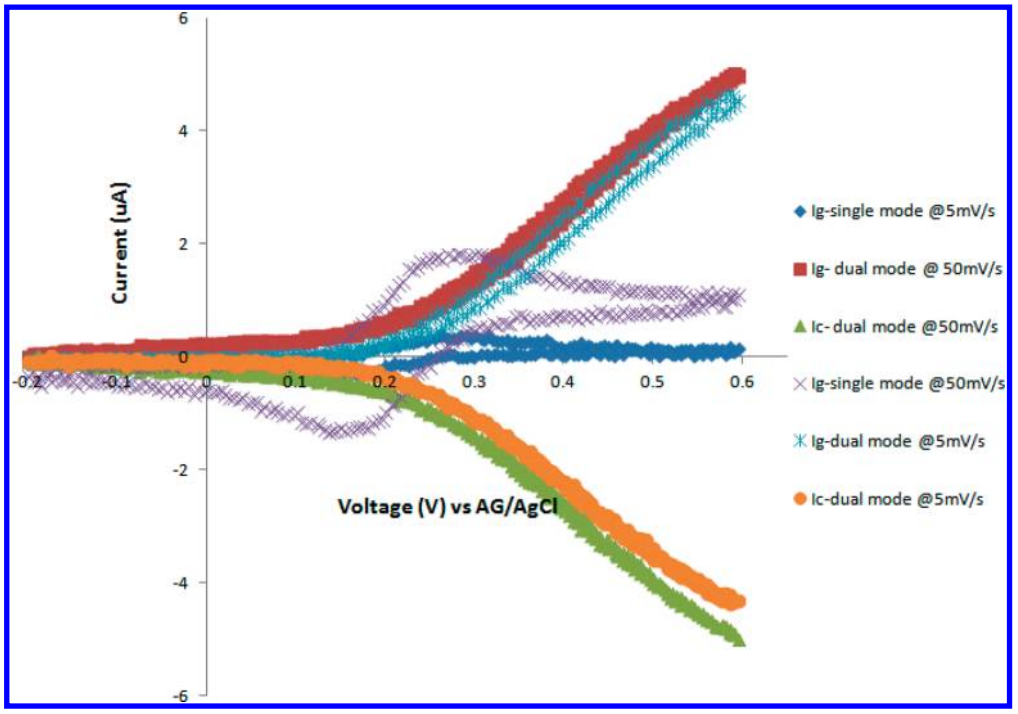

Figure 4. Cyclic voltammograms of 3D carbon IDEAs in 0.5 M KCl and 1 mM $K_4Fe(CN)_6$ solution. IDEA parameter: width/gap, 1.58; height, 1.1 μm. Refer to Table 2 for exact specifications.

efficiencies for different width/gap ratios at a fixed electrode height of 0.22 μm. This height was achieved by pyrolyzing the thinnest SU-8 film (0.6 μm) pattern that we could reliably pattern. We also wanted to test for the maximum amplification that can be reached for the thinnest attainable carbon film. So far, the maximum amplification attained for such carbon IDEAs is 13 (see Figure 3). Table 1 lists the dimensions of the digits before and after pyrolysis used in Figure 3. It can be noted from Table 1 that, as the width/gap ratios increase, the gaps increase only slightly, whereas the widths increase significantly. The significance of increasing the width for improving redox amplification in IDEAs has not been reported yet. The amplification factor as a function of width/gap ratio in Figure 3 shows a steep increase at the higher width/gap ratios. It can also be observed from Figure 3 that the collector efficiency is getting closer to unity for higher width/gap ratios. Our observation for an increase in amplification via an increase in the digit width is explained as follows: The diffusion layer thickness is proportional to the time scale of the experiment as well as the width of the individual digits.[31] As the width of a digit increases, the diffusion layers of individual digits overlap more, and hence, the signal becomes proportional to the surface area of the whole array (keeping number of digits constant) instead of being dependent on the sum of areas of the individual digits. In such a case, the greater the overlap, the smaller is the current signal.[32] In single mode, the potential is only applied to alternate digits; hence, the diffusion layers will show less overlap (say at 5 mV/s) or even none at all (say at 50 mV/s). By widening the digits, we improve the overlap, thereby reducing the signal and improving the amplification as the redox amplification factor is calculated as the ratio of the generator current in dual mode to the generator current in single mode. In dual mode, diffusion layers for consecutive digits more readily overlap. As opposed to single mode where greater overlap causes reduction in signal due to linear diffusion, the greater overlap in dual mode increases current due to redox cycling. Hence, dual mode current is significantly higher for wider electrodes. In summary, increasing the digit width optimizes redox amplification by decreasing the denominator (single mode generator current) and increasing the numerator (dual mode generator current). Even though reducing the gap between electrodes is an important factor in improving redox cycling, it is obvious from these results that one can also focus on increasing the width/gap ratio by increasing width to improve redox cycling. This is especially true in the case of conventional UV photolithography where achieving gaps in the submicrometer range is challenging. For gap spacings where the diffusion profiles already overlap, one expects the amplification factor to increase until an electrode width is reached corresponding to the redox species diffusion length.

Effect of Voltage Sweep Rate on Sensor Performance. In Figure 4, we show CVs at two different potential sweep rates: 5 and 50 mV/s for both single and dual mode operation. At 50 mV/s in single mode, one can see a typical CV curve for a 1 mM $K_4Fe(CN)_6$ solution with both oxidation and reduction peaks visible. A similar CV curve is obtained at 5 mV/s, although with lower current. For CVs that feature peaks, the Randles Sevcik equation holds[33]

$$i = 0.4463nFAC\left(\frac{nFvD}{RT}\right)^{0.5} \quad (3)$$

where n is the number of electrons transferred in the redox event, v is the sweep rate in V/s, R is the ideal gas constant, and T is temperature in K. The rest of the symbols have the same meanings as described for eq 1. It can be seen that the peak current is proportional to the square root of the sweep rate. At higher sweep rates, the rate of consumption of the redox species at the electrode surface is very high, and diffusion from the bulk cannot provide enough mass transport to reach a steady state. Insufficient mass transport causes the current to

dx.doi.org/10.1021/ac4033356 | Anal. Chem. 2014, 86, 2963−2971

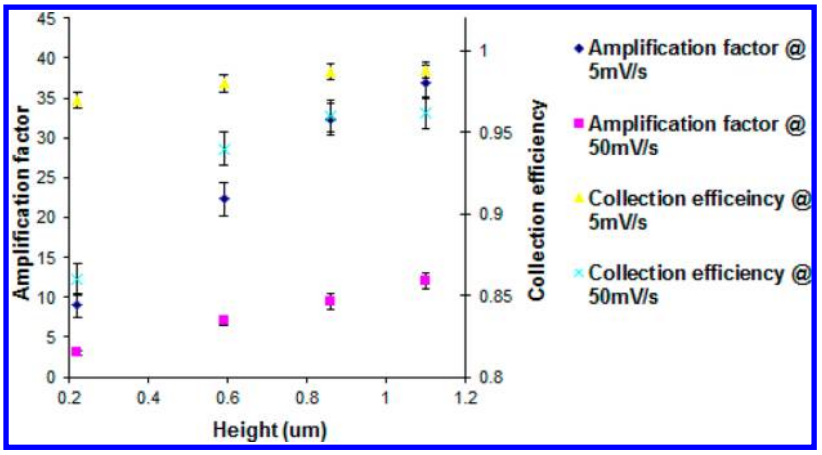

Figure 5. Amplification factor and collection efficiency vs height at a width/gap ratio of 1.6. Refer to Table 2 for dimension details.

peak (eq 3). At lower sweep rates, the rate of consumption of the redox species is lower and the diffusion from the bulk is fast enough to achieve steady state; hence, instead of a redox peak, a diffusion plateau results. Once this steady state regime is reached, the magnitude of the limiting current becomes independent of the sweep rate and relies on the geometry of electrode.[34] The magnitude of this limiting current is much lower compared to the peak current obtained from eq 3 but is still in direct proportion to the concentration of the redox species at the electrode surface. In Figure 4, the peak shaped CVs in single mode at 50 mV/s may be either due to the partial overlap of the diffusion layers or simply because the diffusion layers have not grown wider than the characteristic (smallest) dimension of the individual digits.

In dual mode, the efficient cycling of the redox species between the IDEAs enhances the mass transport to such an extent that the limiting current becomes independent of the sweep rate. The hysteresis between the anodic and the cathodic current in the CV curves is reduced significantly, indicating that steady state is being approached. The CV for both the generator and collector electrodes generally displays a typical sigmoidal shape, although with significantly larger limiting current than in single mode due to redox cycling. This enhanced mass transport by cycling the redox species between IDEAs has an equivalent effect to that of the nonlinear, diffusion contribution in the case of micro electrodes where a sigmoid behavior can be seen even at relatively large sweep rates due to the enhanced mass transport. The current rise to the plateau, in the case of carbon electrodes, is less steep than the case of highly conductive IDEAs. The conductivity of carbon IDEAs is not quite as high as that of noble metals (100S/cm for glassy carbon vs 4×10^5S/cm for Au), and hence, the CV shows an *iR* drop resulting in a current that gradually increases toward the plateau instead of a sharp rise toward the limiting current. Adding *iR* drop effects to the simulations results in a similar CV as observed experimentally with carbon IDEAs.[22]

The generator current in single mode at 50 mV/s is much higher than that at 5 mV/s due to sweep rate dependence. At lower sweep rates, the time available for redox cycling is longer and hence the redox species cycle a greater number of times. Hence, the collection efficiency is higher at lower sweep rates, i.e., 0.97 at 5 mV/s compared to 0.92 at 50 mV/s. As seen from Figure 4, the difference in generator current at 50 and 5 mV/s in single mode is significant, while in dual mode the difference is minimal. In single mode, the current is lower at lower sweep rates, as discussed earlier (refer to eq 3)

Signal Enhancement as a Function of Electrode Height (No Flow). One of the biggest advantages of using SU-8 UV photolithography is that it allows for simpler implementation of high aspect ratio IDEAs. As the height of the electrode increases, the surface area available for redox species to interact with electrodes increases. More importantly, this greater height confines redox species in the trench between the electrodes, allowing for more efficient redox cycling. This phenomenon was experimentally demonstrated by Dam et al.[15] using platinum IDEAs with a height of 7 μm and a gap spacing of 1 μm. The design allowed these authors to reach amplification factors of up to 70. Their experimental results were validated through simulations by Odijk et.al.[29] Through simulations, Kim et.al[35] demonstrated that the diffusion pathways between the vertical walls of the electrodes are linear whereas the diffusion pathways between the horizontal edges are elliptical. Hence, the practical distance for diffusion is shorter for 3D high aspect ratio electrodes. In Figure 5, we see that, at a sweep rate of 5 mV/s, the collection efficiency increases steadily from 0.97 to 0.985 while, with increasing electrode height, the amplification factor increases dramatically from 9 to 37. Our experimental results showed that the difference between the generator and collector current in dual mode was more or less constant at all electrode heights. However, it was observed that the current increased with height which is why an increase in the collection efficiency is observed. This goes to show that one needs to exploit the height of the IDEAs at low sweep rates to get sizable signal enhancement.

Effect of Flow on Redox Cycling for Different Heights and Width/Gap Ratios. It is expected that a solution containing electro-active species flown over an electrode will increase the amperometric signal[34] and IDEAs have also been shown to be extremely efficient in improving the sensitivity of electrochemical detection. It was only natural to combine the two to investigate redox cycling at IDEAs in flow injection analysis[10] and high-performance liquid chromatography.[36,37] The effect of flow on collection efficiency and redox cycling has been studied for planar IDEAs,[11,38] but the effect of flow on 3D IDEAs has not yet been investigated.

In single mode, the current under flow conditions is linearly proportional to the cube root of flow rate as shown in eq 4[34]

dx.doi.org/10.1021/ac4033356 | *Anal. Chem.* 2014, 86, 2963−2971

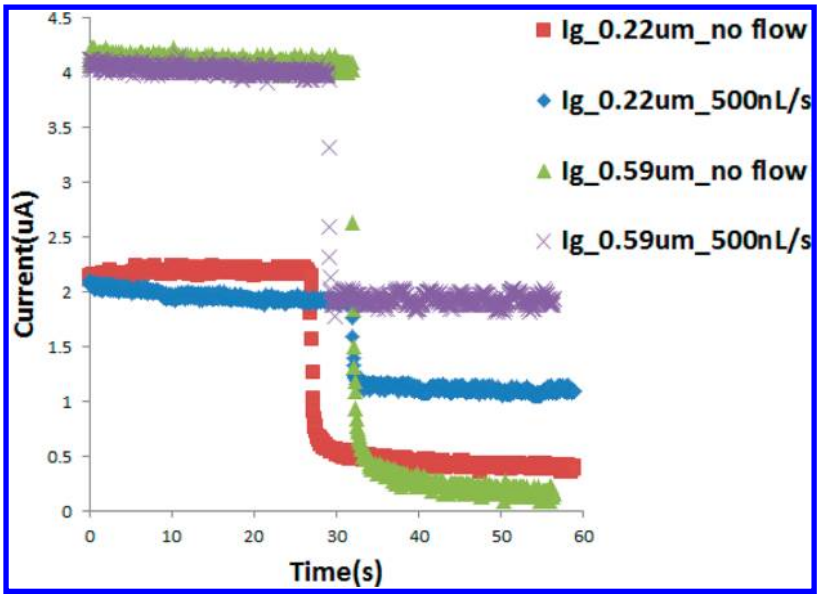

Figure 6. Chromoamperogram of 3D carbon IDEAs under flow and no flow condition for different IDEA heights: 0.22 and 0.59 μm. Generator current was measured in dual mode for approximately 30 s, followed by single mode.

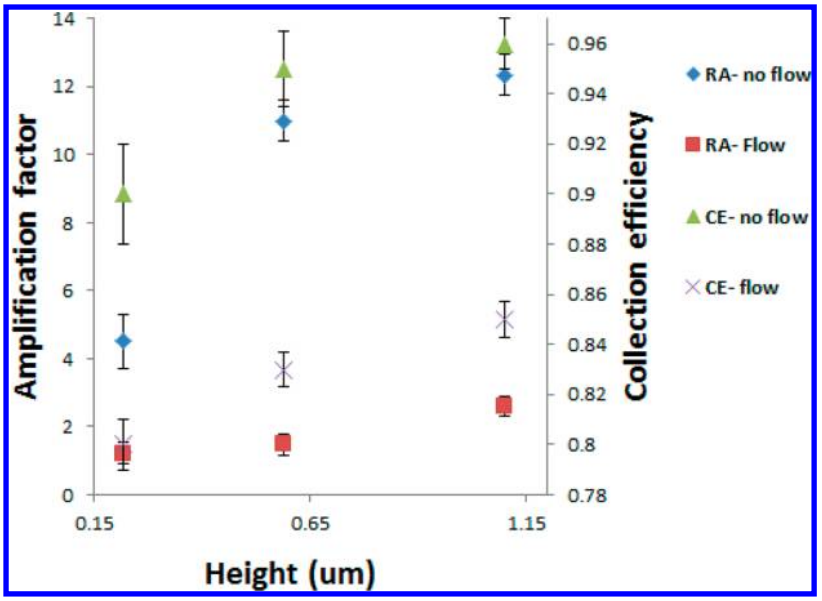

Figure 7. Redox amplification and collection efficiency as a function of height under flow (500 nL/s) and no flow conditions. IDEA width/gap ratio: 1.21.

$$I = 1.47nFC\left(\frac{DA}{B}\right)^{2/3}\nu^{1/3} \quad (4)$$

where B is channel height and the other variables have the same meaning as defined in eqs 1 and 4. Hence, when the IDEA is operated in single mode, we get approximately 7 times higher current under flow (500 nL/s) as compared to the stationary situation demonstrated in Figure 6. The influence of flow in dual mode is somewhat more complicated. It was observed that the generator current in dual mode under flow conditions was smaller than the current under stagnant conditions (refer to Figure 6). The underlying reason is that, in stagnant solutions, and especially for flat IDEAs, elliptical diffusion plays a dominant role in redox cycling. Indeed, under high lateral flow conditions, mass transport is mainly due to lateral convective flow (replacing diffusion from the top in the case of a stagnant solution), elliptical diffusion at the electrode edges, and linear diffusion between the vertical walls of the electrodes. Elliptical diffusion is impeded by the flow as half of the redox species that contribute to redox cycling by elliptical diffusion at the horizontal edges move in the direction of the flow (downstream) and the other half move in the opposite direction (upstream). The redox species that go upstream are impeded by convective flow, reducing the collection efficiency, whereas the species that go downstream are assisted by the flow.[39] This elliptical diffusion effect can be seen from Figure 6, where with an increase in IDEA height, the difference in dual mode generator current between flow and no flow conditions decreases. The difference is 1.5% in taller IDEAs (0.59 μm) vs 12% in shorter IDEAs (0.22 μm). The flow mainly affects elliptical diffusion, which is a dominant factor in redox cycling for shorter IDEAs. With an increase in IDEA height, the linear

dx.doi.org/10.1021/ac4033356 | Anal. Chem. 2014, 86, 2963−2971

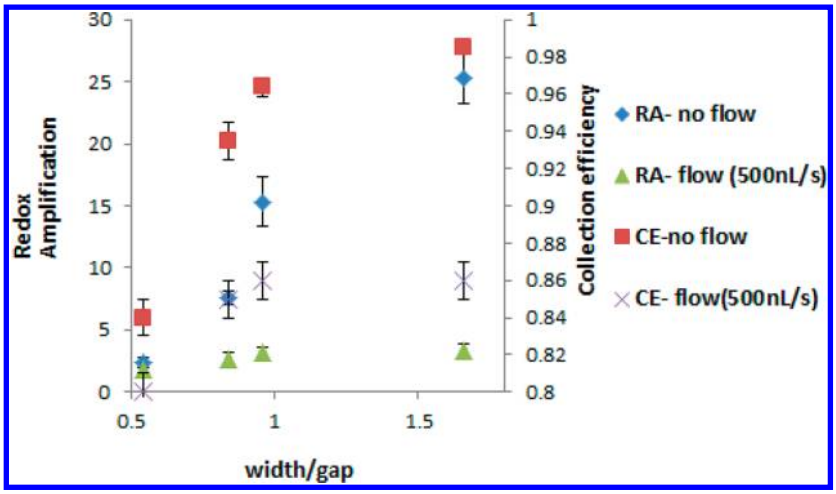

Figure 8. Redox amplification and collection efficiency at flow and no flow conditions vs width/gap ratio. Height = 0.59 μm.

diffusion in redox cycling dominates and the difference in generator current decreases. It can be concluded that the generator current in dual mode under no flow conditions is always higher (refer to Figure 6), whereas the generator current in single mode under flow conditions is higher. Thus, redox amplification decreases under flow.

In Figure 7, we demonstrate the sensor performance under flow at different electrode heights and observe that there is a steeper increase in amplification for taller IDEAs (slope of 2 from 0.59 to 1.1 μm) compared to shorter ones (slope of less than 1 from 0.22 to 0.59 μm). This data suggests that, with a further increase in IDEA height, the detrimental effect of flow on redox cycling will continue to diminish. The result falls in line with our explanation about how flow mostly affects elliptical diffusion. The effect of flow wears off with the increase in IDEA height, where linear diffusion starts to dominate.

As evident from Figure 8, the width/gap ratio has very little impact on redox amplification under a high flow rate of 500 nL/s. Under flow conditions, the amplification factor increases marginally as the width/gap ratio is increased. For the lowest width/gap, the amplification factor is only 1.8, whereas it is 3.4 for the highest ratio. As explained above, these low values of redox amplification are due to the poor collection efficiency at a flow rate of 500 nL/s. We also learned that, to achieve better collection efficiencies, the mass transport due to convection needs to be reduced.[11]

Detection Limit. Since the dependence of redox amplification and collection efficiency on IDEA geometry, sweep rate, and flow conditions has been established, the next step is to find out the detection limit for our 3D IDEAs. The detection limit was found for our best IDEAs under no flow conditions. It can be seen that current exhibits linearity with respect to an analyte concentration between 1 μM and 10 mM (Figure 9). The slope corresponds to a sensitivity of 5.8 nA/μM. The average noise signal in single and dual mode corresponds to 1 nA. The detection limit calculated using 3σ/m criteria corresponds to 0.5 μM.

Currently, our best electrodes are the ones with the width/gap ratio of 1.58 (see Table 2) and height of 1.1 μm that provides amplification factor of 37. This factor is half of the maximum amplification factor recorded for the 3D platinum IDEAs, i.e., 74 by Dam et al. The group used platinum electrodes which had height of 7 μm and width of 2 μm, with a gap of 1 μm at the top. To achieve amplification similar to the

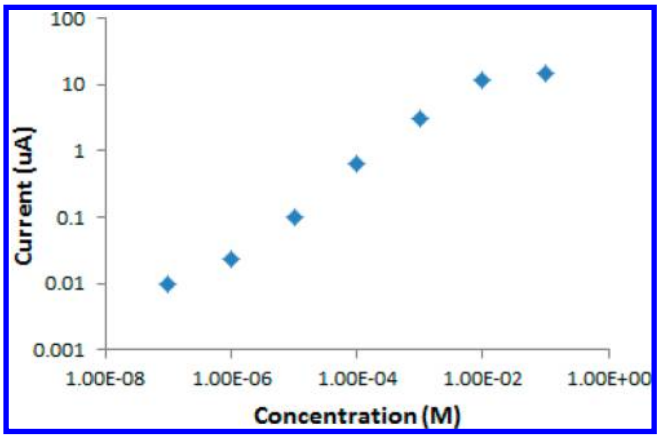

Figure 9. Redox cycling current as a function of the concentration of the $K_4Fe(CN)_6$ in 0.5 M KCl at the IDEA with a width/gap ratio of 1.58 and height of 1.1 μm.

one achieved by Dam et al., the height of 3D carbon IDEAs needs to be increased. Predicting the exact height required to achieve a factor of 70 is not intuitive as the amplification does not linearly increase with height for 3D carbon IDEAs. This is mainly because the digit side wall profile varies with different heights. Also, it will require further optimization of photolithography parameters to completely resolve the same gap spacings at higher SU-8 heights, which may be extremely difficult using conventional UV lithography. The fabrication of 3D platinum electrodes by Dam et al. requires steps such as reactive ion etching, metal evaporation, and lift-off, whereas we have demonstrated a much simpler method to fabricate 3D IDEAs.

CONCLUSION

Our work has demonstrated that 3D carbon IDEAs can be reliably fabricated using conventional UV photolithography followed by pyrolysis to obtain high redox amplification factors. By reducing the UV exposure dosage and increasing PEB time at lower bake temperatures, submicrometer gap spacings are attainable for heights of up to 5.1 μm for SU-8 patterns. Amplification can be enhanced by increasing the electrode width and height, keeping the gap spacing the same, and by using the simple, less expensive technique described above. Performance of the 3D carbon IDEAs was tested using a

dx.doi.org/10.1021/ac4033356 | Anal. Chem. 2014, 86, 2963−2971

standard redox probe, $K_4Fe(CN)_6$, for different IDEA parameters such as width/gap ratio and height in both flow and no flow conditions. 3D carbon IDEAs demonstrated greater signal enhancement at higher width/gap ratios for submicrometer gaps. Under no flow conditions, redox amplification increased significantly with increasing height. The effect of sweep rate on amplification was studied, and it was found that, at lower sweep rates, redox amplification was higher due to improved collection efficiency, even though the limiting currents remained unaffected. Under flow conditions, signal enhancement was lower because flow is detrimental to elliptical diffusion between the horizontal edges of IDEAs. With an increase in height, the contribution from linear diffusion between the vertical walls increased, improving redox amplification.

It was demonstrated that a simple, conventional photolithography technique can yield high performance carbon IDEAs. Even though this fabrication technique shows limitations in reducing the gap size, it compensates by providing significant electrode height to yield high redox amplification factors.

AUTHOR INFORMATION

Corresponding Author

*E-mail: kamathr@uci.edu.

Notes

The authors declare no competing financial interest.

ACKNOWLEDGMENTS

Authors would like to acknowledge Giulia Canton for technical assistance in SEM imaging and Alexandra Perebikovsky for assisting with the Table of Contents graphic.

REFERENCES

(1) Bakker, E.; Qin, Y. *Anal. Chem.* **2006**, *78*, 3965−3984.
(2) Coetzee, J. F. *Pure Appl. Chem.* **1986**, *58*, 1091−1104.
(3) Yang, C.; Huang, Y.; Hassler, B. L.; Worden, R. M.; Mason, A. J. *IEEE Trans. Biomed. Circuits Syst.* **2009**, *3*, 160−168.
(4) Janata, J. *Principles of Chemical Sensors*; Springer: Dordrecht, Heidelberg, London, New York, 2009; pp 207−208.
(5) Goda, T.; Singi, A. B.; Maeda, Y.; Matsumoto, A.; Torimura, M.; Aoki, H.; Miyahara, Y. *Sensors (Basel)* **2013**, *13*, 2267−2278.
(6) Zimmerman, W. B. *Chem. Eng. Sci.* **2011**, *66*, 1412−1425.
(7) Takenaka, S. In *Electrochemistry of Nucleic Acids and Proteins, Towards Electrochemical Sensors for Genomics and Proteomics*; Paleček, E., Scheller, F., Wang, J., Eds.; Elsevier: New York, 2005; Volume *1*, pp 345−367.
(8) Paleček, E.; Jelen, F. In *Electrochemistry of Nucleic Acids and Proteins, Towards Electrochemical Sensors for Genomics and Proteomics*; Paleček, E., Scheller, F., Wang, J., Eds.; Elsevier: New York, 2005; Volume *1*, pp 73−173.
(9) Xia, F.; Jin, W.; Yin, X.; Fang, Z. *J. Chromatogr., A* **2005**, *1063*, 227−233.
(10) Niwa, O. *Electroanalysis* **1995**, 606−613.
(11) Bjorefors, F.; Standman, C.; Nyholm, L. *Electroanalysis* **2000**, *12*, 255−261.
(12) Rahimi, M.; Mikkelsen, S. R. *Anal. Chem.* **2011**, *83*, 7555−7559.
(13) Goluch, E. D.; Wolfrum, B.; Singh, P. S.; Zevenbergen, M. A. G.; Lemay, S. G. *Anal. Bioanal. Chem.* **2009**, *394*, 447−456.
(14) Yang, X.; Zhang, G. Diffusion-Controlled Redox Cycling at Nanoscale Interdigitated Electrodes. In *Proceedings of the COMSOL Multiphysics User's Conference*; COMSOL, Inc.: Burlington, MA, 2005.
(15) Dam, V. A. T.; Olthuis, W.; van den Berg, A. *Analyst* **2007**, *132*, 365−370.
(16) Aoki, K. *J. Electroanal. Chem.* **1988**, *256*, 269−282.
(17) Niwa, O.; Morita, M.; Tabei, H. *Anal. Chem.* **1990**, *175*, 447−452.
(18) Niwa, O.; Xu, Y.; Halsall, H. B.; Heineman, W. R. *Anal. Chem.* **1993**, *65*, 1559−1563.
(19) Ueno, K.; Hayashida, M.; Ye, J.-Y.; Misawa, H. *Electrochem. Commun.* **2005**, *7*, 161−165.
(20) Cohen, A. E.; Kunz, R. R. *Sens., Actuators, B: Chem.* **2000**, *62*, 23−29.
(21) Singh, K. V.; Whited, A. M.; Ragineni, Y.; Barrett, T. W.; King, J.; Solanki, R.. *Anal. Bioanal. Chem.* **2010**, *397*, 1493−1502.
(22) Heo, J. I.; Shim, D. S.; Teixidor, G. T.; Oh, S.; Madou, M. J.; Shin, H. *J. Electrochem. Soc.* **2011**, *158*, J76−80.
(23) Oesch, U.; Janata, J. *Electrochim. Acta* **1983**, *28*, 1247−1253.
(24) Ranganathan, S.; McCreery, R.; Majji, S. M.; Madou, M. *J. Electrochem. Soc.* **2000**, *147*, 277.
(25) Taylor, R. J.; Humffray, A. A. *J. Electroanal. Chem. Interfacial Electrochem.* **1973**, *42*, 347−354.
(26) Keller, S.; Blagoi, G.; Lillemose, M.; Haefliger, D.; Boisen, A. *J. Micromech. Microeng.* **2008**, *18*, 125020.
(27) Mardegan, A.; Kamath, R.; Sharma, S.; Scopece, P.; Ugo, P.; Madou, M. *J. Electrochem. Soc.* **2013**, *160*, B132−B137.
(28) Martinez-Duarte, R.; Renaud, P.; Madou, M. J. *Electrophoresis* **2011**, *32*, 2385−2392.
(29) Odijk, M.; Olthuis, W.; Dam, V. A. T.; van den Berg, A. *Electroanalysis* **2008**, *20*, 463−468.
(30) Iwasaki, Y.; Morita, M. *Curr. Sep.* **1995**, 2−8.
(31) Tomčík, P. *Sensors (Basel)* **2013**, *13*, 13659−13684.
(32) Stulik, K.; Amatore, C.; Holub, K.; Marecek, V.; Kutner, W. Ł. O. *Pure Appl. Chem.* **2000**, *72*, 1483−1492.
(33) Zanello, P. *Inorganic Electrochemistry: Theory, Practice, and Application*; Royal Society of Chemistry: London, 2003; p 606.
(34) Bard, A. J.; Faulkner, L. R.; Swain, E.; Robey, C. *Electrochemical Methods: Fundamentals and Applications*; John Wiley & Sons, Inc: New York, 2001; p 448 and 813.
(35) Kim, S. K.; Hesketh, P. J.; Li, C.; Thomas, J. H.; Halsall, H. B.; Heineman, W. R. *Biosens. Bioelectron.* **2004**, *20*, 887−894.
(36) Takahashi, M.; Morita, M.; Niwa, O.; Tabei, H. *J. Electroanal. Chem.* **1992**, *335*, 253−263.
(37) Takahashi, M.; Morita, M.; Niwa, O.; Tabei, H. *Sensors (Basel)* **1993**, *14*, 336−339.
(38) Niwa, O.; Morita, M. *Anal. Chem.* **1996**, 355−359.
(39) Alden, J. A.; Compton, R. G. *J. Electroanal. Chem.* **1996**, *415*, 1−12.